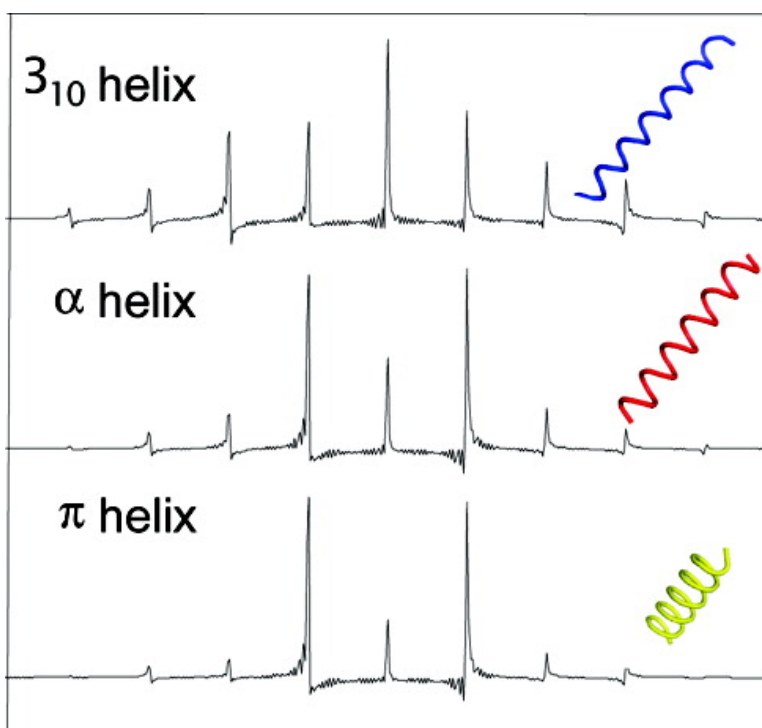


Determination of Peptide Backbone Torsion Angles Using Double-Quantum Dipolar Recoupling Solid-State NMR Spectroscopy

Manish A. Mehta, Matthew T. Eddy, Seth A. McNeill, Frank D. Mills, and Joanna R. Long

J. Am. Chem. Soc., **2008**, 130 (7), 2202-2212 • DOI: 10.1021/ja074244w

Downloaded from <http://pubs.acs.org> on February 8, 2009



More About This Article

Additional resources and features associated with this article are available within the HTML version:

- Supporting Information
- Links to the 2 articles that cite this article, as of the time of this article download
- Access to high resolution figures
- Links to articles and content related to this article
- Copyright permission to reproduce figures and/or text from this article



[View the Full Text HTML](#)



Determination of Peptide Backbone Torsion Angles Using Double-Quantum Dipolar Recoupling Solid-State NMR Spectroscopy

Manish A. Mehta,^{*,†} Matthew T. Eddy,[†] Seth A. McNeill,[‡] Frank D. Mills,[‡] and Joanna R. Long^{*,‡}

Department of Chemistry and Biochemistry, 119 Woodland Street, Oberlin College, Oberlin, Ohio 44074, and Department of Biochemistry and Molecular Biology and McKnight Brain Institute, University of Florida, Gainesville, Florida 32610

Received June 25, 2007; E-mail: manish.mehta@oberlin.edu; jrlong@mbi.ufl.edu

Abstract: Several approaches for utilizing dipolar recoupling solid-state NMR (ssNMR) techniques to determine local structure at high resolution in peptides and proteins have been developed. However, many of these techniques measure only one torsion angle or are accurate for only certain classes of secondary structure. Additionally, the efficiency with which these dipolar recoupling experiments suppress the deleterious effects of chemical shift anisotropy (CSA) at high magnetic field strengths varies. Dipolar recoupling with a windowless sequence (DRAWS) has proven to be an effective pulse sequence for exciting double-quantum (DQ) coherences between adjacent carbonyl carbons along the peptide backbone. By allowing this DQ coherence to evolve, it is possible to measure the relative orientations of the CSA tensors and subsequently use this information to determine the Ramachandran torsion angles ϕ and ψ . Here, we explore the accuracies of the assumptions made in interpreting DQ-DRAWS data and demonstrate their fidelity in measuring torsion angles corresponding to a variety of secondary structures irrespective of hydrogen-bonding patterns. It is shown how a simple choice of isotopic labels and experimental conditions allows accurate measurement of backbone secondary structures without any prior knowledge. This approach is considerably more sensitive for determining structure in helices and has comparable accuracy for β -sheet and extended conformations relative to other methods. We also illustrate the ability of DQ-DRAWS to distinguish between structures in heterogeneous samples.

1. Introduction

Solid-state NMR (ssNMR) is unique in its ability to measure at atomic level resolution structure and dynamics in large protein complexes using in situ conditions. In particular, the ability to study protein structure and dynamics in heterogeneous systems at atomic resolution provides exciting opportunities for determining the relationship between structure and function in native matrices such as lipid bilayers and spider silk as well as non-native environments such as on polymer surfaces.^{1–5} Gaining insights into the structure and dynamics of membrane-associated proteins in their native lipid environment is necessary for understanding both the functional mechanisms of these proteins and the importance of membrane fluidity, individual lipids, fatty acids, and small molecules in protein function.^{6,7} Magic angle spinning (MAS) ssNMR has also proven to be uniquely

applicable to studying of amyloid fibril formation, examining peptide binding to nanoparticles, and examining the structure and dynamics of proteins adsorbed on inorganic substrate.^{8–13}

In recent years, much of the focus in the biomolecular ssNMR community has been on developing MAS methodologies for global determination of protein structure.^{14–21} These studies have primarily utilized multidimensional ssNMR experiments to

[†] Oberlin College.

[‡] University of Florida.

- (1) Marassi, F. M.; Ramamoorthy, A.; Opella, S. J. *Proc. Natl. Acad. Sci. U.S.A.* **1997**, *94*, 8551–8556.
- (2) Lange, A.; Giller, K.; Hornig, S.; Martin-Eauclaire, M. F.; Pongs, O.; Becker, S.; Baldus, M. *Nature* **2006**, *440*, 959–962.
- (3) van Beek, J. D.; Hess, S.; Vollrath, F.; Meier, B. H. *Proc. Natl. Acad. Sci. U.S.A.* **2002**, *99*, 10266–10271.
- (4) van Beek, J. D.; Beaulieu, L.; Schafer, H.; Demura, M.; Asakura, T.; Meier, B. H. *Nature* **2000**, *405*, 1077–1079.
- (5) Long, J. R.; Oyler, N.; Drobny, G. P.; Stayton, P. S. *J. Am. Chem. Soc.* **2002**, *124*, 6297–6303.

- (6) Mani, R.; Cady, S. D.; Tang, M.; Waring, A. J.; Lehrert, R. I.; Hong, M. *Proc. Natl. Acad. Sci. U.S.A.* **2006**, *103*, 16242–16247.
- (7) Yang, J.; Gabrys, C. M.; Weliky, D. P. *Biochemistry* **2001**, *40*, 8126–8137.
- (8) Petkova, A. T.; Leapman, R. D.; Guo, Z. H.; Yau, W. M.; Mattson, M. P.; Tycko, R. *Science* **2005**, *307*, 262–265.
- (9) Petkova, A. T.; Ishii, Y.; Balbach, J. J.; Antzutkin, O. N.; Leapman, R. D.; Delaglio, F.; Tycko, R. *Proc. Natl. Acad. Sci. U.S.A.* **2002**, *99*, 16742–16747.
- (10) Heise, H.; Hoyer, W.; Becker, S.; Andronesi, O. C.; Riedel, D.; Baldus, M. *Proc. Natl. Acad. Sci. U.S.A.* **2005**, *102*, 15871–15876.
- (11) Bower, P. V.; Louie, E. A.; Long, J. R.; Stayton, P. S.; Drobny, G. P. *Langmuir* **2005**, *21*, 3002–3007.
- (12) Drobny, G. P.; Long, J. R.; Shaw, W. J.; Cotton, M.; Stayton, P. S. *Encyclopedia of NMR*; Grant, D. M., Harris, R. K., Eds.; John Wiley: Chichester, New York, 2002; Vol. 9.
- (13) Drobny, G. P.; Long, J. R.; Karlsson, T.; Shaw, W.; Popham, J.; Oyler, N.; Bower, P.; Stringer, J.; Gregory, D.; Mehta, M.; Stayton, P. S. *Annu. Rev. Phys. Chem.* **2003**, *54*, 531–571.
- (14) Zech, S. G.; Wand, A. J.; McDermott, A. E. *J. Am. Chem. Soc.* **2005**, *127*, 8618–8626.
- (15) Castellani, F.; van Rossum, B.; Diehl, A.; Schubert, M.; Rehbein, K.; Oschkinat, H. *Nature* **2002**, *420*, 98–102.
- (16) Castellani, F.; van Rossum, B. J.; Diehl, A.; Rehbein, K.; Oschkinat, H. *Biochemistry* **2003**, *42*, 11476–11483.

determine through-space and through-bond interactions, much like high-resolution NMR studies of soluble proteins. The success of this approach relies on obtaining hundreds or thousands of constraints for even small proteins, and these studies have been particularly successful for nanocrystalline samples. When a protein exists in an array of structures or in an extended-type structure, these measurements are not able to determine structure as accurately. Samples created by fibrillarization, freezing, or lyophilization have also been studied,^{8,9,22} but quite often their resolution is compromised due to line broadening from side-chain conformational variability as well as other inhomogeneous broadening mechanisms, making spectral assignments untenable.

When samples have unresolved resonances or higher-resolution structural information is needed to answer mechanistic questions, coherent measurements can be used to obtain quantitative distances between specific atoms in order to refine an extended structure or to determine conformational heterogeneity. A variety of MAS ssNMR methods have been developed to extract information about local atomic structure in noncrystalline, macroscopically disordered proteins.^{13,23,24} Given the large proton homonuclear dipolar couplings, these methods typically rely on the spin characteristics of rare spin- $1/2$ nuclei, such as ^{13}C and ^{15}N , either in concert with each other or with their directly bonded protons, invariably requiring the incorporation of isotopically enriched amino acids. Extracting backbone secondary structure information can be accomplished by measuring internuclear spin interactions. NMR experiments that focus on internuclear distances^{25–27} or the relative orientations of the dipolar interactions^{28–32} and/or relative chemical shift anisotropies^{21,33–41} (CSAs) of particular spin networks have

been developed and demonstrated to measure backbone secondary structure in peptides and proteins. However, many of these experiments have only been tested on a small subset of model compounds with known secondary structures and then applied to unoriented or noncrystalline compounds which are, through independent experiments, known to fall into secondary structure regimes particularly relevant to the experiment and/or isotopic labeling scheme selected. Each method has its advantages and drawbacks, yet what is desirable is an experiment that can be used to discern the full range of secondary geometries and which retains a consistent accuracy over that range. This approach should evaluate interactions which are relatively free of experimental parameters requiring time-intensive independent measurements (such as relaxation, chemical shift anisotropy orientations, and radio frequency (rf) field homogeneity) or assumptions about the generality of a particular parameter. Additionally, for systems in which no prior structural information is available or which have a mixture of conformations, consideration of the labeling schemes and pulse sequences applicable to a wide array of secondary structures is required. To our knowledge, no sequence has demonstrated the ability to retain its accuracy over a broad range of secondary structures; in fact, many are known to be relevant for extended or β -sheet-type secondary structures and are of limited accuracy for turns and helices.^{21,28–31,40,41}

This work addresses the experimental accuracy and relevance of using $^{13}\text{C}'(i) \rightarrow ^{13}\text{C}'(i+1)$ interactions to determine backbone torsion angles. This particular pair of spins was chosen due to their ease of isotopic enrichment, consistent relaxation and CSA characteristics, the sufficiently large size of their interactions, and the lack of redundancy in their relative CSA orientations over the allowed ϕ , ψ torsion angle space.^{5,13,33–36} Thus, determining structures within both helices and more extended conformations should be possible. The DQ-DRAWS experiment (chosen to select $^{13}\text{C}'(i) \rightarrow ^{13}\text{C}'(i+1)$ interactions) offers a robust technique for examining these interactions without detrimental effects to biological NMR samples even at high fields and with currently achievable rf fields and spinning speeds.²⁷ Since these are homonuclear interactions, two-spin coherences can be DQ filtered, an advantage which obviates corrections for single quantum interactions from naturally abundant ^{13}C nuclei with overlapping resonances.^{5,42,43}

The overriding goal of this work is to demonstrate that with only three types of well-established parameters, $^{13}\text{C}'$ isotropic chemical shifts, peptide bond lengths, and peptide bond angles, one can utilize DQ-DRAWS experiments to determine backbone torsion angles in proteins with high accuracy—regardless of the underlying secondary structure of the system or protein being studied. To this end, a series of tripeptides with published crystal structures spanning a variety of torsion angles and with varying hydrogen-bonding patterns was selected for study. A total of ten compounds were chosen, three with torsion angles typical for helices, two with torsion angles typical for extended conformations, one with torsion angles similar to a β -sheet, one with torsion angles commonly seen in a turn conformation, and three with torsion angles intermediate between classical α -helix

- (17) Igumenova, T. I.; McDermott, A. E.; Zilm, K. W.; Martin, R. W.; Paulson, E. K.; Wand, A. J. *J. Am. Chem. Soc.* **2004**, *126*, 6720–6727.
- (18) Franks, W. T.; Wylie, B. J.; Stellfox, S. A.; Rienstra, C. M. *J. Am. Chem. Soc.* **2006**, *128*, 3154–3155.
- (19) Franks, W. T.; Zhou, D. H.; Wylie, B. J.; Money, B. G.; Graesser, D. T.; Frericks, H. L.; Sahota, G.; Rienstra, C. M. *J. Am. Chem. Soc.* **2005**, *127*, 12291–12305.
- (20) Wylie, B. J.; Sperling, L. J.; Frericks, H. L.; Shah, G. J.; Franks, W. T.; Rienstra, C. M. *J. Am. Chem. Soc.* **2007**, *129*, 5318–5319.
- (21) Rienstra, C. M.; Hohwy, M.; Mueller, L. J.; Jaroniec, C. P.; Reif, B.; Griffin, R. G. *J. Am. Chem. Soc.* **2002**, *124*, 11908–11922.
- (22) Havlin, R. H.; Tycko, R. *Proc. Natl. Acad. Sci. U.S.A.* **2005**, *102*, 3284–3289.
- (23) Luca, S.; Heise, H.; Baldus, M. *Acc. Chem. Res.* **2003**, *36*, 858–865.
- (24) Tycko, R. *Annu. Rev. Phys. Chem.* **2001**, *52*, 575–606.
- (25) Gregory, D. M.; Mitchell, D. J.; Stringer, J. A.; Kiihne, S.; Shiels, J. C.; Callahan, J.; Mehta, M. A.; Drobny, G. P. *Chem. Phys. Lett.* **1995**, *246*, 654–663.
- (26) Ishii, Y. *J. Chem. Phys.* **2001**, *114*, 8473–8483.
- (27) Karlsson, T.; Popham, J. M.; Long, J. R.; Oyler, N.; Drobny, G. P. *J. Am. Chem. Soc.* **2003**, *125*, 7394–7407.
- (28) Reif, B.; Hohwy, M.; Jaroniec, C. P.; Rienstra, C. M.; Griffin, R. G. *J. Magn. Reson.* **2000**, *145*, 132–141.
- (29) Hong, M.; Gross, J. D.; Griffin, R. G. *J. Phys. Chem. B* **1997**, *101*, 5869–5874.
- (30) Ladizhansky, V.; Veshort, M.; Griffin, R. G. *J. Magn. Reson.* **2002**, *154*, 317–324.
- (31) Costa, P. R.; Gross, J. D.; Hong, M.; Griffin, R. G. *Chem. Phys. Lett.* **1997**, *280*, 95–103.
- (32) Feng, X.; Eden, M.; Brinkmann, A.; Luthman, H.; Eriksson, L.; Graslund, A.; Antzutkin, O. N.; Levitt, M. H. *J. Am. Chem. Soc.* **1997**, *119*, 12006–12007.
- (33) Tycko, R.; Weliky, D. P.; Berger, A. E. *J. Chem. Phys.* **1996**, *105*, 7915–7930.
- (34) Weliky, D. P.; Tycko, R. *J. Am. Chem. Soc.* **1996**, *118*, 8487–8488.
- (35) Bower, P. V.; Oyler, N.; Mehta, M. A.; Long, J. R.; Stayton, P. S.; Drobny, G. P. *J. Am. Chem. Soc.* **1999**, *121*, 8373–8375.
- (36) Blanco, F. J.; Tycko, R. *J. Magn. Reson.* **2001**, *149*, 131–138.
- (37) Gabrys, C. M.; Yang, J.; Weliky, D. P. *J. Biomol. NMR* **2003**, *26*, 49–68.
- (38) Hong, M.; Gross, J. D.; Hu, W.; Griffin, R. G. *J. Magn. Reson.* **1998**, *135*, 169–177.
- (39) Gregory, D. M.; Mehta, M. A.; Shiels, J. C.; Drobny, G. P. *J. Chem. Phys.* **1997**, *107*, 28–42.
- (40) Hong, M.; Griffin, R. G. *Biophys. J.* **1998**, *74*, A296–A296.

- (41) Chan, J. C. C.; Tycko, R. *J. Am. Chem. Soc.* **2003**, *125*, 11828–11829.
- (42) Gregory, D. M.; Wolfe, G. M.; Jarvie, T. P.; Shiels, J. C.; Drobny, G. P. *Mol. Phys.* **1996**, *89*, 1835–1849.
- (43) Long, J. R.; Shaw, W. J.; Stayton, P. S.; Drobny, G. P. *Biochemistry* **2001**, *40*, 15451–15455.

Table 1. Structural Data for Tripeptides Based on Published X-ray Structures

peptide	reference	ω (deg)	ϕ (deg)	ψ (deg)	$C'(i) \rightarrow C'(i+1)$ distance (Å) ^a	calculated distance (Å) ^b
GAV	Chaturvedi (1991) ⁴⁴	-171.3	-68.7	-38.1	3.064	3.079
GAF	Ramasubbu (1989) ⁴⁵	-173.7	-71.2	-33.4	3.134	3.096
GGV	Lalitha (1984) ⁴⁶	-175.7	-77.0	-22.3	3.162	3.143
AGG	Lalitha (1985) ⁴⁷		-83	169	3.192	3.196
FAG	Parthasarathy (1993) ⁴⁸	-174.8	-96.7	-46.3	3.341	3.320
AFG	Parthasarathy (1993) ⁴⁸	177.7	-98.1	-65.2	3.366	3.329
GFF	Precigoux (1986) ⁴⁹	-177.0	-126.2	-55.7	3.542	3.539
GFG	Go (1995) ⁵⁰	-175.4	-126.3	132.0	3.523	3.539
VGG	Lalitha (1986) ⁵¹	-179.4	-155.1	154.7	3.641	3.675
AAA	Fawcett (1975) ⁵²	175.2	-145.7	145.5	3.634	3.684

^a Distance reported between C' atoms in the first and second amino acids. ^b Predicted distances based on published ϕ torsion angles and canonical bond lengths and angles.⁵³

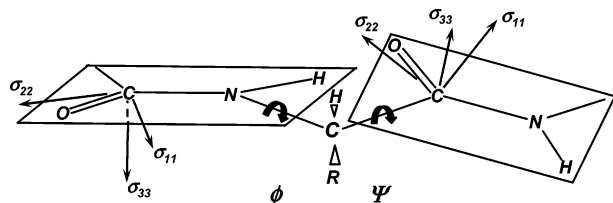


Figure 1. Mutual orientation of two-peptide planes described by torsion angles ϕ and ψ , which characterize different secondary structures. Principal values of the CSA tensor, σ_{ii} , are shown in the molecular frame. The distance between the C' atoms is solely dependent on the three bond lengths between them, their bond angles, and the torsion angle ϕ .

and β -sheet values (Table 1). In addition to providing a test bed for measuring the accuracy of torsion angle measurements, information from these compounds can add to the knowledge base of isotropic and anisotropic chemical shifts for $^{13}C'$ spins in proteins. The methods outlined are not only relevant to measuring structure in well-ordered systems but can also be used to provide insight into the structures and relative proportions in heterogeneous conformations. While the compounds in this study were crystallized for comparison with X-ray crystallography, results have previously demonstrated that neither a high degree of macroscopic ordering nor the attendant line-narrowing are requirements for the backbone torsion angle measurements or for distinguishing multiple conformations.⁵

In his seminal paper on peptide backbone secondary structure, Pauling described the hybrid character of the amide bond and its planar geometry (Figure 1).⁵⁴ This electronic structure has direct impact on the individual chemical shift anisotropies of the $^{13}C'$ atoms and their orientations relative to the amide bonds in which they participate. Namely, their CSAs are significantly more asymmetric and larger than those of the C_{α} and aliphatic carbons in proteins and their spans are on the order of 150 ppm

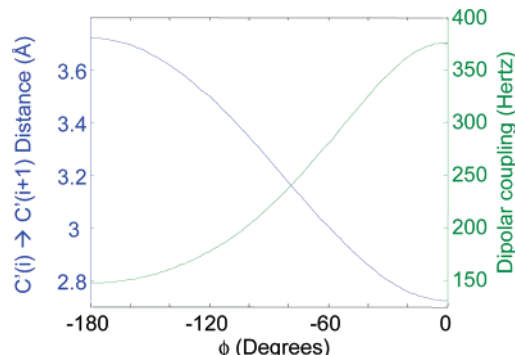


Figure 2. Predicted intercarbonyl distances (blue) and dipolar couplings (green) as a function of the torsion angle ϕ .

with σ_{11} and σ_{33} being largely invariant.^{55–60} Changes in the backbone torsion angles associated with the adoption of a particular secondary structure lead to changes in σ_{22} and consequently the isotropic chemical shift.^{57–59,61} Of specific importance to this work is that the sp^2 character of the amide bond causes the $^{13}C'$ CSA to have a particular orientation relative to its planar peptide bond; namely, σ_{11} and σ_{22} lie in the plane of the amide bond and σ_{33} is perpendicular to it and σ_{11} is oriented 34 – 47° relative to the C–N bond.^{57,62} Thus, if one assumes the amide bond to be planar and determines the ϕ torsion angle from the distances between the $^{13}C'$ atoms (Figure 2), one can extrapolate the torsion angle ψ by measuring the relative CSA orientations of the $^{13}C'$ nuclei in adjacent amino acids. This measurement is readily accomplished by exciting a DQ coherence between the $^{13}C'(i)$ and $^{13}C'(i+1)$ nuclei and allowing it to evolve before converting the magnetization back to an observable state. However, variability in the orientation of the $^{13}C'$ CSAs relative to their peptide planes and nonplanarity of the amide bonds may vitiate the result. By selecting several compounds with ω deviating from -180° by as much as 8.7° and with varying hydrogen-bonding patterns, we have investigated the overall accuracy of using dipolar coupling DQ

- (44) Chaturvedi, S.; Go, K.; Parthasarathy, R. *Biopolymers* **1991**, *31*, 397–407.
 (45) Ramasubbu, N.; Parthasarathy, R. *Biopolymers* **1989**, *28*, 1259–1269.
 (46) Lalitha, V.; Subramanian, E.; Bordner, J. *Int. J. Pept. Protein Res.* **1984**, *24*, 437–441.
 (47) Lalitha, V.; Subramanian, E.; Bordner, J. *Indian J. Pure Appl. Phys.* **1985**, *23*, 506–508.
 (48) Parthasarathy, R.; Go, K.; Chaturvedi, S. *Biopolymers* **1993**, *33*, 163–171.
 (49) Precigoux, G.; Cotrait, M.; Geoffre, S. *Acta Crystallogr.: Sect. C* **1986**, *42*, 315–317.
 (50) Go, K.; Parthasarathy, R. *Biopolymers* **1995**, *36*, 607–614.
 (51) Lalitha, V.; Murali, R.; Subramanian, E. *Int. J. Pept. Protein Res.* **1986**, *27*, 472–477.
 (52) Fawcett, J. K.; Camerman, N.; Camerman, A. *Acta Crystallogr.: Sect. B* **1975**, *B 31*, 658–665.
 (53) Engh, R. A.; Huber, R. *Acta Crystallogr.: Sect. A* **1991**, *47*, 392–400.
 (54) Pauling, L.; Corey, R. B.; Branson, H. R. *Proc. Natl. Acad. Sci. U.S.A.* **1951**, *37*, 205–211.

- (55) Stark, R. E.; Jelinski, L. W.; Ruben, D. J.; Torchia, D. A.; Griffin, R. G. *J. Magn. Reson.* **1983**, *55*, 266–273.
 (56) Ando, S.; Yamanobe, T.; Ando, I.; Shoji, A.; Ozaki, T.; Tabeta, R.; Saito, H. *J. Am. Chem. Soc.* **1985**, *107*, 7648–7652.
 (57) Oas, T. G.; Hartzell, C. J.; Memahon, T. J.; Drobny, G. P.; Dahlquist, F. W. *J. Am. Chem. Soc.* **1987**, *109*, 5956–5962.
 (58) Asakawa, N.; Kuroki, S.; Kurosu, H.; Ando, I.; Shoji, A.; Ozaki, T. *J. Am. Chem. Soc.* **1992**, *114*, 3261–3265.
 (59) Wei, Y. F.; Lee, D. K.; Ramamoorthy, A. *J. Am. Chem. Soc.* **2001**, *123*, 6118–6126.
 (60) Hartzell, C. J.; Whitfield, M.; Oas, T. G.; Drobny, G. P. *J. Am. Chem. Soc.* **1987**, *109*, 5966–5969.
 (61) Cornilescu, G.; Bax, A. *J. Am. Chem. Soc.* **2000**, *122*, 10143–10154.
 (62) Teng, Q.; Iqbal, M.; Cross, T. A. *J. Am. Chem. Soc.* **1992**, *114*, 5312–5321.

coherence between adjacent $^{13}\text{C}'$ nuclei to determine ϕ and applying the relative orientations of the $^{13}\text{C}'$ CSAs to determine ψ .

Given the dependence of the $^{13}\text{C}'$ σ_{22} elements on secondary structure, it is possible to observe different conformations for particular $^{13}\text{C}'$ nuclei as different isotropic chemical shifts in a ^{13}C MAS spectrum. For the 2D DQ-DRAWS experiment a corollary exists in the second dimension; namely, differences in secondary structure lead to differences in the $^{13}\text{C}'$ sum CSA tensor and therefore different isotropic resonances and intensities for the spinning sidebands. Thus, 2D DQ-DRAWS allows the clear distinction of multiple conformations and the determination of their corresponding backbone torsion angles (vide infra).

2. Experimental Methods

Samples. All tripeptides were made using established Fmoc protocols on an Applied Biosystems peptide synthesizer utilizing chlorotrityl resins with the carboxy terminal amino acid attached (Novabiochem). Isotopically enriched Fmoc amino acids were synthesized starting with $^{13}\text{C}'$ -enriched amino acids (Cambridge Isotope Laboratories, Inc.) and using established synthesis procedures.⁶³ After the solid-phase synthesis, peptides were cleaved with 95%:5%:: CH_2Cl_2 :TFA and filtered, and the solvent was removed under vacuum. Then crude peptides were brought up in acetic acid and loaded onto Dowex resin, from which, after several water washes, the samples were eluted with 1% ammonium hydroxide and purity was verified by TLC and size exclusion chromatography. The doubly- ^{13}C -labeled tripeptides were dissolved in water with their unlabeled counterparts (purchased from Bachem when possible) at a 1:9::labeled:unlabeled ratio and recrystallized by slow evaporation at room temperature. Finally, the resulting crystals were ground and analyzed by powder diffraction prior to the NMR experiments. The NMR samples consisted of approximately 25 mg each (2.5 mg of labeled sample or <5 μmole of each spin).

X-ray Powder Diffraction. The crystallinity and space group of each of the labeled NMR samples were checked using X-ray powder diffraction. Powder diffraction measurements were made on each of the crystalline NMR samples using a continuous scan from 5° to 50° in increments of 0.03° in 2θ using a Philips MPD-3040 X-ray Powder Diffractometer. The X-ray beam had a wavelength of 1.54 \AA from a Cu α source. Single-crystal X-ray structures for each of the tripeptides were obtained from the Cambridge Crystallographic Structural Database. CrystalMaker and CrystalDiffract were used to compare the collected powder pattern for each peptide to that predicted from the known crystal structure in order to confirm that the correct crystalline polymorph had been grown for each tripeptide.

NMR Spectroscopy. Measurements on all samples were carried out on a custom assembled NMR spectrometer with a Discovery console (Tecmag; Houston, TX), 14.1 T magnet (Magnex; Oxford, England), and a 39-channel matrix shim system (Resonance Research, Inc.; Billerica, MA), operating at a proton frequency of 600.377 MHz (150.987 MHz for ^{13}C). A doubly tuned 4 mm magic angle spinning probe (Doty Scientific; Columbia, South Carolina) was employed. The rotor speed was regulated to ± 3 Hz for all MAS experiments, and experiments were performed at room temperature. To ensure high homogeneity in the applied rf field, samples were confined to the innermost 5 mm of the rotor. Pulse widths were determined by performing a nutation experiment with the spectrometer frequency set to the center of one of the two carbonyl resonances; after cross polarization, a pulse of increasing duration was applied for up to 70 μs . The modulation in the signal intensity of the resonance was then fit to an exponentially damped cosine function, and the period of that

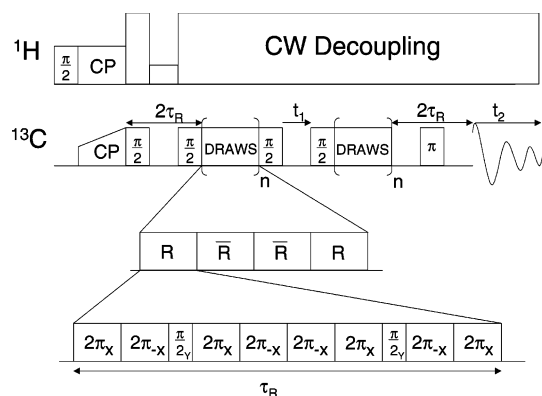


Figure 3. Pulse sequence diagram for the DQ-DRAWS experiment. The DQ coherence is created before the t_1 period, allowed to evolve during t_1 , and then converted back to observable signal after t_1 . For DQ buildup curves, t_1 is held to zero, and n is incremented from 1 to 10. In the 2D DQ-DRAWS experiment, n is held fixed (usually between 4 and 6), and t_1 is incremented to yield a 2D data set. The rotor is spun at the magic angle, with the spin rate matched to the rf, 8.5ν (MAS) = ν (rf). Cross-polarization is denoted by CP, R is the basic DRAWS pulse block, and \bar{R} represents R with all pulse phases shifted by π . A 16-step phase cycle is used to select the DQ coherence pathway.

function was subsequently used to determine the 90° , 180° , and 360° pulse widths (7.1, 14.2, and 28.4 μs , respectively). This rf field ensured at least a 3:1 mismatch between the ^{13}C and ^1H fields during the windowless DRAWS sequence. CP/MAS spectra were collected using a 2 ms cross polarization contact time and 120 kHz ^1H CW decoupling. A 20% ramp was applied on the ^{13}C channel during cross polarization. A Hahn echo sequence, $\tau_r - \pi - \tau_r$, was used after cross polarization and before acquisition to reduce the background carbon signal from the probe materials. Each transient was collected with a sweep width of 50 kHz and 20 ms of acquisition (1024 points). Spectra were collected at spinning speeds of 3, 4, and 5 kHz to determine the principal values of the individual carbonyl carbon chemical shift anisotropy tensors.

For the DQ-DRAWS experiments (Figure 3), the rotor frequency was set such that the rotor period equaled 8.5 rf periods, or 241.4 μs (4142 Hz). The buildup experiments were performed with 1200–1600 transients per point, and the 2D DQ experiments were collected in two different manners using States–Haberkorn–Ruben phase sensitive detection (the 16-step phase cycle is given in the Supporting Information). In the first approach, spectra were collected in t_1 at a rate of 10 spectra per rotor period, and sample collection (128 transients per point) was carried out for more than 6 ms to generate a full 2D data set without any linear prediction. In the second approach, 40 spectra (512 transients per spectrum) were collected over the course of one rotor period in t_1 . The full pulse sequence is given in Figure 3. In order to determine the DQ coherence excitation efficiencies, an unfiltered spectrum was collected for each compound by removing only the dipolar recoupling portion of the pulse sequence. Signal intensities were determined by integrating the isotropic carbonyl resonances and their attendant spinning sidebands. The DQC excitation efficiency is given by the ratio of the signal in the DQ-filtered spectrum with the most signal to the unfiltered spectrum, corrected for the ^{13}C natural abundance contribution.

For some compounds, data were also obtained at 500 MHz using a Bruker DRX spectrometer, 42.5 kHz ^{13}C rf field, 110 kHz ^1H decoupling, and a 5 kHz spinning speed. While the 600 MHz data were collected with many transients to provide clarity in presentation, data at 500 MHz were collected with only 256 transients per spectrum and acquisition of a full set of CP/MAS, DQ buildup, and 2D DQ data required less than 16 h.

Data Analysis. Principal values of the chemical shift tensors of the labeled carbonyl carbons in each tripeptide were determined using CP/MAS spectra collected at 3, 4, and 5 kHz sample spinning. Intensities

(63) Samuel-Landtiser, M.; Zachariah, C.; Williams, C. R.; Edison, A. S.; Long, J. R. *Current Protocols in Protein Science*; Coligan, J. E., Dunn, B. M., Speicher, D. W., Wingfield, P. T., Eds.; John Wiley and Sons, Inc.: Brooklyn, NY, 2007; Vol. 26.3, pp 1–49.

of the spinning sidebands from -4 to $+4$ in the CP/MAS spectra were integrated. The integrated intensities were fit to the principal values of the chemical shift tensor using a full density matrix numerical simulation to take into account finite pulse length effects. The principal values of the chemical shift tensors determined for each carbonyl carbon were later used in the simulations of the corresponding DQ experiments for each sample.

Distances between adjacent carbonyl carbons were determined by a least-squares fit of DQ buildup curves to numerical simulations. In these simulations, the single quantum relaxation values were held at 50 Hz based on an independent measurement of the typical carbonyl carbon T_2 for the rf fields used in these experiments. The only parameter varied in the simulations was the distance between the two atoms and the corresponding change in the ϕ torsion angle (see comments below regarding iterative fitting). The torsion angle ϕ , assumed to be negative, was calculated using the interatomic distance and canonical values of peptide bond lengths and bond angles;⁵³ a distinction in the values was made for compounds in which glycine versus other amino acids occupied the $(i + 1)$ position.

Relative orientations between $^{13}\text{C}'$ spins as well as with the dipolar coupling interaction were calculated by orienting each individual $^{13}\text{C}'$ CSA relative to its respective amide bond, setting the ω torsion angle to 180° , varying the ϕ torsion angle $\pm 10^\circ$ in 5° increments from the value obtained by fitting the DQ buildup data, and varying the ψ angle in 2° increments over the accessible space (180° to -180°). To orient the CSAs in the molecular frame, standard bond lengths and angles were used to set the atomic coordinates of the backbone atoms for a given conformation.⁵³ The CSAs were then oriented relative to the peptide amide bonds with δ_{11} and δ_{22} lying in the peptide plane and δ_{33} orthogonal to them. Previous studies have shown δ_{11} lies at an angle of $34\text{--}47^\circ$ relative to the C–N bond, dependent on the conformation and hydrogen bonding of the particular peptide carbonyl carbons examined.^{55,57,62} For the simulations, we examined orientations varying from 37 to 42° . Numerical simulations of the 2D DQ evolution for each set of torsion angles were compared to experimental data. Relative χ^2 values were determined as described by Gabrys et al.;³⁷ 2D contour maps showing fits within 2σ of the χ^2 minimum are given in the Supporting Information. The second derivative of the χ^2 map while holding either ϕ constant (and fitting ψ) or ψ constant (and fitting ϕ) was used to determine the best fit and standard deviation for the ϕ, ψ torsion angles. χ^2 maps were generated using both a point by point comparison in t_1 and by comparing the intensities of the Fourier components (which are increments of the spinning speed) for the experimental and simulated t_1 data; these maps are provided in the Supporting Information. Additional coarse-grained maps over wider areas are also provided, demonstrating that even without prior knowledge of the torsion angle ϕ , 2D DQ-CSA measurements can accurately measure backbone torsion angles.

Computer Simulations. Simulations incorporating full, time-dependent density matrix equations were performed using SIMPSON⁶⁴ and compiled Matlab codes. These calculations incorporate finite pulses, the magic angle spinning speed, frequency offsets, individual CSA principle values, and relative orientations of the carbonyl carbon CSAs and the dipolar coupling vector. Fits of the DQ buildup data and 2D DQ evolution data were done iteratively. First the distance between the $^{13}\text{C}'$ atoms was determined using simulations in which the ϕ, ψ torsion angles were assumed. This distance was used to fit an approximate value for the torsion angle ϕ . This torsion angle was then input with the full range of ψ values ($-180^\circ \rightarrow +180^\circ$) into the 2D DQ simulations to find a rough fit of the data (at this point, torsion angles usually fit within 20° of the expected values). Once these values were known, the DQ buildup data were refit using these torsion angles to orient the CSA and dipolar coupling tensors. This final value of ϕ

was then used in setting up the grid of ϕ, ψ torsion angles for the final fit of the 2D DQ data. The final grid consisted of ϕ values within 10° of the DQ buildup value incremented in 5° steps and ψ values incremented from -180° to 180° in 2° steps.

Pulse sequences (Bruker, Tecmag) and files for simulating 2D DQ-CSA data with Simpson are available on request (Matlab, c++).

3. Results

X-ray Powder Diffraction. The powder diffraction patterns were simulated for each compound from the published crystal coordinates and compared to experimental data in order to ensure the same crystalline form. For all compounds, the spectra were in qualitative agreement with the simulations.

CSA Measurements. Results for the measurements of $^{13}\text{C}'$ CSA tensors are presented in Table 2. Chemical shifts were referenced relative to neat TMS under MAS (2.0 ppm).⁶⁵ Principal values are reported as the average and standard deviation from measurements at 3, 4, and 5 kHz MAS. As δ_{iso} varies with amino acid sequence, backbone conformation and hydrogen-bond length, the δ_{22} element is most affected; however, smaller, linear dependencies of δ_{11} and δ_{33} with δ_{iso} are also seen. These trends are in good agreement with previously reported results.⁵⁹

Double Quantum Buildup Experiments. Computer simulations of the experimental data incorporating the chemical shift anisotropies, CSA orientations determined from the 2D experiment (see below) and a 50 Hz $T_{2\text{sq}}$ relaxation rate for each spin minimized distances to within 0.04 \AA of the X-ray values (0.03 \AA rmsd) and 0.06 \AA (0.04 \AA rmsd) of distances calculated using the published torsion angles and assuming canonical bond lengths and bond angles;⁵³ no further parameters (such as damping functions) were needed to fit the data. The standard deviations were determined by taking the second derivative of the χ^2 plots. The ϕ torsion angles calculated from these distances have a rmsd of 4° relative to torsion angle values reported for published X-ray structures (Table 1). For each sample, the integrated intensity of the DQ-filtered spectrum with the greatest signal was compared to the intensities of the two labeled carbonyls in a CP/MAS experiment collected at the same spinning speed and rf fields to determine the efficiency of the DQ excitation. Double-quantum excitation efficiencies ranged from 19 to 22% as predicted by computer simulations incorporating the experimental dipolar couplings, CSAs, and rf fields. Experimental data and simulations for three representative peptides along with χ^2 analyses are shown in Figure 4. Results of the DQ-buildup experiments for all ten samples are listed in Table 2.

2D DQ Experiments. Two-dimensional DQ evolution data were collected in two manners for each of the tripeptides. In the first approach, hypercomplex quadrature data in the second dimension were collected over a t_1 period of a single rotor cycle with 40 real and 40 imaginary data points evenly spaced over the rotor period. Using a small number of t_1 data points allowed for a larger number of transients to be collected in a given period of time and ensured that all the data points had high signal intensities since little relaxation is observed over this time period. In the second set of experiments, t_1 data were collected at a rate of 10 real and imaginary data points per rotor period out to 25–30 rotor periods (>6 ms) to generate a well-resolved two-

(64) Bak, M.; Rasmussen, J. T.; Nielsen, N. C. *J. Magn. Reson.* **2000**, *147*, 296–330.

(65) Morcombe, C. R.; Zilm, K. W. *J. Magn. Reson.* **2003**, *162*, 479–486.

Table 2. Results of NMR Measurements on Tripeptides

peptide	δ_{iso}^a (ppm)	δ_{11} (ppm)	δ_{22} (ppm)	δ_{33} (ppm)	$\Delta\sigma^b$ (ppm)	η^c	distance ^d (Å)	ϕ^e (deg)	ψ^f (deg)
*G*AV	168.43	247.8 (1.0)	166.1 (3.2)	91.2 (3.1)	156.6	0.94	3.10(0.01)	-71.8(1.4)	-30.3(0.5)
	175.22	240.6 (0.5)	193.5 (2.5)	91.5 (2.2)	149.1	0.56		-70.6(0.6)	-31.6(0.4)
*G*AF	170.86	245.6(1.7)	177.16(3.0)	89.8(2.3)	155.9	0.84	3.12(0.01)	-73.3(1.3)	-31.7(1.0)
	176.44	248.2 (1.5)	191.04(1.1)	90.0 (1.0)	158.2	0.66		-82.8(2.0)	-30.9(1.6)
*G*GV	171.1	243.2 (2.3)	179.5 (2.2)	90.5 (0.7)	152.7	0.79	3.20(0.01)	-83.9(1.4)	-26.5(3.3)
*A*GG	172.76	243.4(1.8)	180.8(1.7)	94.2(0.2)	149.2	0.80	3.15(0.01)	-78.0(1.4)	154.1(5.7)
	170.98	243.5(1.9)	177.8(1.9)	91.7(0.7)	151.8	0.83		-78.4(2.5)	155.1(5.5)
*F*AG	170.37	245.3(0.8)	175.8(2.9)	90.1(2.4)	155.2	0.87	3.31(0.01)	-96.2(1.4)	85.6(7.6)
	174.74	242.5(1.2)	192.2(2.5)	89.3(1.4)	153.2	0.59		-96.0(2.0)	-65.7(5.6)
*A*FG	171.18	247.0(1.1)	174.9(2.5)	91.7(1.4)	155.3	0.91	3.37(0.01)	-103.3(1.4)	90.2(8.0)
	173.04	239.4(0.4)	188.7(0.8)	90.9(0.4)	148.5	0.62		-94.5(2.7)	98.2(5.5)
								-102.4(3.8)	-66.8(4.3)
*G*FF	166.73	246.8(0.1)	160.6(1.3)	92.7(1.3)	154.2	0.85	3.52(0.01)	-124.2(1.7)	-67.7(5.7)
	174.01	244.7(1.9)	185.7(3.6)	91.7(1.6)	153.0	0.72		-95.7(6.7)	95.7(6.7)
*G*FG	167.46	255.7(4.0)	167.2(5.0)	79.6(1.1)	176.1	0.99	3.49(0.01)	-118.6(1.7)	-54.8(2.8)
	172.56	232.6(1.1)	186.5(0.3)	98.7(0.8)	133.9	0.62		-125.6(2.1)	-54.9(2.5)
*V*GG	169.73	243.6(2.7)	176.3(2.5)	89.2(0.3)	154.4	0.84	3.69(0.02)	-131.7(4.3)	-69.7(3.9)
	172.31	244.9(1.9)	178.3(1.4)	93.7(0.5)	151.2	0.85		-121.2(3.2)	120.1(5.0)
								-115.4(4.0)	115.4(4.0)
*A*AA	170.98	241.6 (2.4)	178.9(1.2)	92.5(1.2)	149.1	0.80	3.64(0.01)	-144.4(3.4)	-69.4(3.9)
								-160.5(4.3)	141.9(5.0)

^a Chemical shifts for first two ¹³C spins as marked. ^b $\Delta\sigma = \delta_{11} - \delta_{33}$. ^c η as defined by the Haeberlen convention. ^d From DQ buildup experiments. ^e First value determined from DQ buildup distance. Second (and third) value based on two-parameter (ϕ, ψ) fit of 2D DQ-CSA. ^f Value(s) of ψ corresponding to first ϕ value determined by fitting 2D DQ-CSA data with ϕ held to DQ buildup value and ψ freely varied. Values of ψ reported with second (and third) ϕ value determined using a two-parameter fit of the 2D DQ-CSA data with ϕ varying within 10° of the DQ buildup value and ψ varying from -180° to +180°. Standard deviations are given in parentheses.

dimensional spectrum and allow the determination of the DQ linewidths. In all the crystalline samples, signal was observed for even the longest t_1 time points. The spectra were numerically simulated over a range of ϕ, ψ torsion angles as described above, and a least-squares fit of the data yielded a single pair of torsion angles within 15° of the torsion angles (8° rmsd) measured via X-ray for six of the compounds; four of the compounds minimized to two possible conformations, one of which was in agreement with the crystallographic values. Particularly accurate, unique fits were obtained for the samples with torsion angles similar to helices. Simulations were compared to experimental data in three ways: (1) by a direct comparison of t_1 data collected over one rotor cycle to simulated t_1 data, (2) by a direct comparison of t_1 data collected over 6–8 ms with simulated t_1 data damped by T_2^* relaxation, and (3) by determining the Fourier components at integers of the spinning speed for t_1 data collected over one rotor period to Fourier components of the simulated t_1 data. All three approaches gave qualitatively similar torsion angle fits. However, the Fourier component analysis gave the most accuracy and is less affected by experimental linewidths or resonance offsets. Projections of the DQ dimension along with best fit simulations (approach 2) are shown for the three tripeptides, GGV, GFF, and VGG, in Figure 5. A fit of the data for GGV using all three approaches is shown in Figure 6. The results for all 10 tripeptides are summarized in Table 2. When comparing each simulation to the experimental data, the scatter, or noise, in the experimental data was minimal. Thus, the uncertainty associated with the simulations can dominate. It was assumed that the mean-squared uncertainty was the same for each data point and could be due to either uncertainty in the experiment or the simulation. Over

the grid of possible (ϕ, ψ) combinations the global χ^2 minimum was found and normalized based on the number of data points being fit (we assumed experimental noise to be random) (see Figure 7). The normalized χ^2 values obtained for other conformations were then compared to the global minimum, and local minima within two standard deviations of the global minimum were considered possible conformations. In only four of the ten sets of experimental data was a second local minimum found. This method is similar to one described in Welicky et al.³⁷

4. Discussion

To a good approximation, the DQ spectrum can be seen to arise from the tensorial sum of the two chemical shift tensors of the interacting ¹³C spins.¹³ For two adjacent ¹³C spins along a peptide backbone, the sum CSA can be expressed as $\sigma_{\text{DQ}} \cong \sigma_1 + R(\phi, \psi) \cdot \sigma_2 \cdot R^T(\phi, \psi)$, in a common frame of reference for the principal axis system of one of the shift tensors. The rotation matrix $R(\phi, \psi)$ transforms the second shift tensor into the principal frame of the first, encoded by the Ramachandran torsion angles (ϕ, ψ). In the language of average Hamiltonian theory, the validity of this approximation lies in the ability of the experiment to remove higher-order terms in the final average Hamiltonian. A full, accurate description of the DQ spectrum requires either a numerical simulation or an average Hamiltonian treatment. However, the sum CSA (σ_{DQ}) can be used to understand the qualitative features of the DQ spectrum, and to quickly discern the secondary structure. The contour plot in the center of Figure 8 displays the span ($\Delta\sigma_{\text{DQ}} = |\sigma_{\text{DQ},33} - \sigma_{\text{DQ},11}|$) for the left half of the Ramachandran angle space (the plot is symmetric about the center). This contour plot of the sum CSA

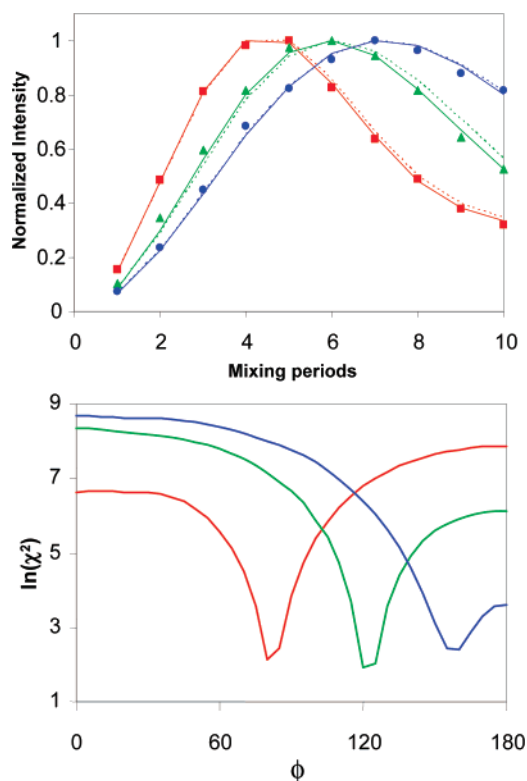


Figure 4. (Top) Experimental (points) and simulated (lines) DQ-DRAWS buildup curves for the tripeptides *G*GV (red ■), *G*FF (green ▲), and *V*GG (blue ●). The normalized signal is plotted as a function of mixing time (1 period is approximately 1 ms). The noise in the experimental data points (i.e., error bar) is smaller than the size of the symbols, and is typically 2% of the signal or less. The experimentally determined values of ϕ are given in Table 2. Solid lines are the best-fit simulations after iterative fitting of the torsion angles. Dashed lines are simulations for the same torsion angle ϕ but with the torsion angle ψ set incorrectly (to $\psi = 0^\circ$). (Bottom) χ^2 analyses of experimental data for GG (red curve), GF (green curve) and VG (blue curve) with simulations as a function of the torsion angle ϕ (ψ held to the experimentally determined value).

span was generated using typical values of $^{13}\text{C}'$ chemical shift anisotropies, canonical orientations of the chemical shift tensors in the molecular frame, and an asymmetry parameter $\eta = 0.80$.

The plot shows regions of low DQ anisotropy (<100 ppm) near the center and regions of large DQ anisotropy (>200 ppm) in the corner regions. Flanking the contour plot are the experimental and simulated DQ spectra for four of the tripeptides: GFG, AAA, FAG, and AFG. The envelope of spinning sidebands in the pure DQ spectrum can be seen to arise from the sum of the CSA tensors in a common frame of reference. The two panels on the left side are GFG and AAA data, two peptides which have extended structures with ϕ measurements of -119° for GFG and -144° for AAA. The DQ spectrum of AAA shows the largest DQ anisotropy, around ~ 266 ppm (40 kHz at 150 MHz). At ($\phi = -144^\circ$, $\psi = 156^\circ$) the sum CSA contour plot predicts a span of 260–270 ppm, which is in good agreement with the spectrum. The configuration of the peptide GFG is not as extended as for AAA, with $\phi = -119^\circ$, $\psi = 120^\circ$, and qualitatively, the breadth of the sideband envelope in the DQ spectrum is not as large as for AAA, which is consistent with a lower contour level (~ 190 ppm) of the sum CSA span on the contour plot at these torsion angles. The DQ spectra on the right are the peptides FAG and AFG, which crystallize in an even less extended conformation; subsequently, their DQ anisotropy is noticeably smaller. Both FAG and AFG

have intermediate values of ϕ (-96° and -103° , respectively), and on the sum CSA surface their coordinates are on about the same contour level (120 ppm). A visual examination of the sideband pattern for FAG and AFG shows a smaller and roughly equal DQ anisotropy. These four tripeptides from our overall set serve to illustrate the utility of the sum CSA and provide useful juxtapositions and contrasts in their DQ spectra and secondary structures.

Due to the lack of symmetry in the $^{13}\text{C}'$ CSAs, determination of backbone torsion angles based on their relative orientations is not hampered by as many multiple minima in the χ^2 fitting over the Ramachandran space as techniques which utilize dipole–dipole interactions. Techniques which rely on the orientation of dipolar tensors are especially prone to multiple minima for nonsheet conformations, hampering their application to systems with helical conformations.^{28–31} The use of DQ buildup experiments to determine ϕ further constrains the fitting of 2D DQ-CSA data. Nonetheless, for ϕ values near -95° there exist multiple solutions of ψ for particular $\Delta\sigma_{\text{DQ}}$ measurements. This is borne out by fits of the data collected for AFG and FAG, which had multiple minima. However, for other values of ϕ , the variation of $\Delta\sigma_{\text{DQ}}$ with ψ is much greater, as is evident in Figure 9. In particular, regions in the Ramachandran plot near canonical helical and sheet structures show a high sensitivity for $\Delta\sigma_{\text{DQ}}$ on both ϕ and ψ .

The DQ sum CSA contour plot in Figure 8 is a qualitative guide to help discern secondary structure from the DQ spectrum. For a more accurate picture, a contour map should be generated using actual shift tensor parameters. The topography of the sum CSA surface over the Ramachandran angles varies noticeably in the closed regions, depending on the shift tensor parameters used for the individual $^{13}\text{C}'$ spins; however, it tends to be less sensitive to such variations in the extended regions. This should not be conflated with the accuracy of the overall DQ method, which is uniform over all regions.

In order to achieve more quantitative agreement between torsion angles derived from simulations of the DQ buildup and 2D DQ-CSA spectra and values from X-ray crystal structures, several quantities were adjusted both in setting up the experiments and in simulating the data. Of key importance to the accuracy of the DQ buildup data is that the ^{13}C rf fields be very homogeneous and that the proton decoupling field be at least 2.5 times greater than the $^{13}\text{C}'$ field during the DRAWS mixing periods. Since DRAWS is a rotor-synchronous sequence, the spinning speed must match the condition $\nu_{\text{RF}} = 8.5 \nu_{\text{rotor}}$.²⁵ Therefore, with an upper limit for the decoupling field for the MAS probe employed of 110 kHz, the spinning speed was limited to a maximum of ~ 5 kHz in order to fulfill both the ^{13}C – ^1H mismatch condition and the rotor synchronization requirement. A slightly more conservative MAS rate of 4.1 kHz was chosen, which proved to be effective for the 2D DQ-CSA data to have several strong sideband intensities to better differentiate secondary structures. The 35 kHz ^{13}C rf field was adequate to cover the range of frequencies needed to suppress the CSAs during the preparation of DQ coherence. Additionally, two methods of decoupling were used: during the mixing periods continuous wave decoupling was applied, but during acquisition phase modulated decoupling using the SPINAL64⁶⁶

(66) Fung, B. M.; Khitrin, A. K.; Ermolaev, K. *J. Magn. Reson.* **2000**, *142*, 97–101.

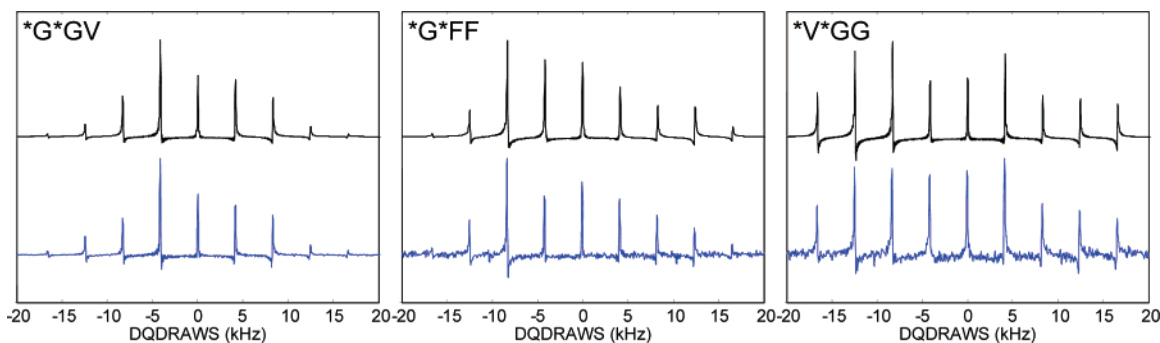


Figure 5. Experimental (lower trace) and simulated (upper trace) DQ projections of 2D DQ-DRAWS spectra of model tripeptides *G*GV (left), *G*FF (middle), and *V*GG (right).

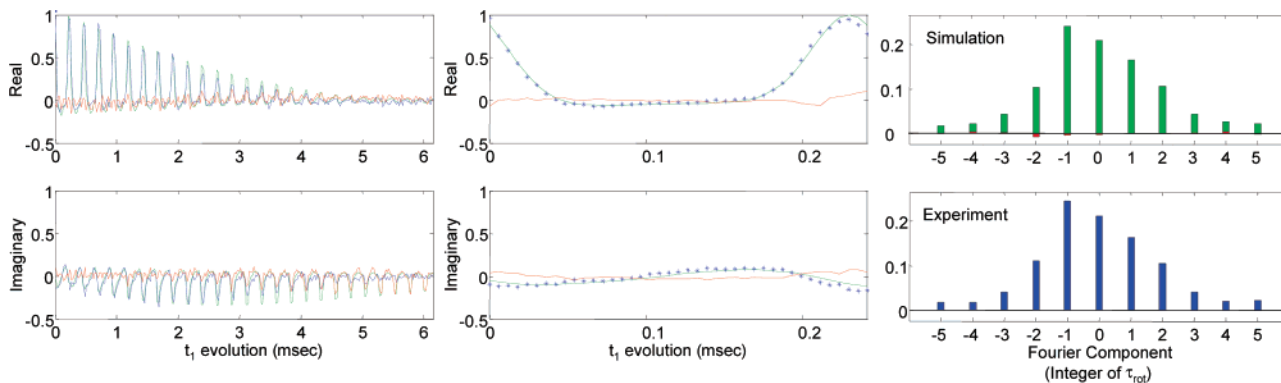


Figure 6. Comparison of three approaches for collecting and simulating experimental data. Experimental data are shown in blue, simulated data are shown in green, and the residuals are shown in red. (Left) Collection of t_1 data for several msec, 10 points per rotor period, plot of integrated intensity for each t_1 timepoint. A 70 Hz damping function was applied to the simulated data. (Middle) Collection of 40 t_1 time points (real and imaginary) in one rotor period (241 μ s). (Right) Calculated Fourier components at integers of the spinning speed for t_1 data collected over a single rotor period.

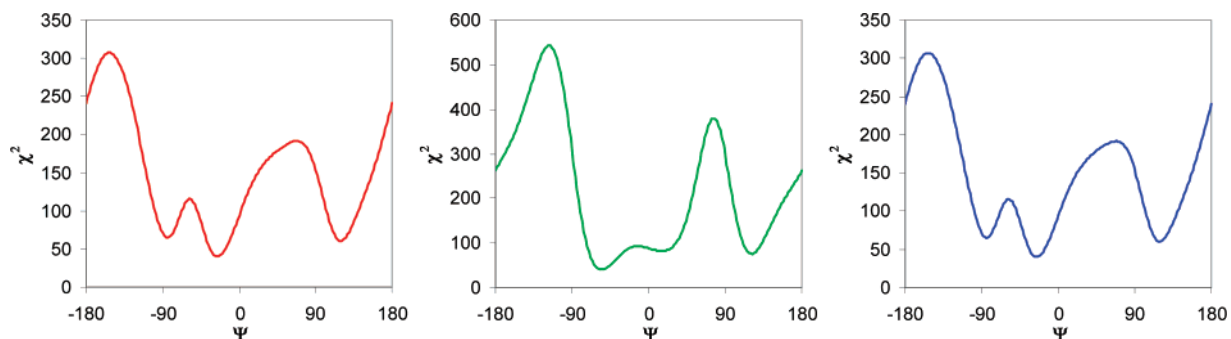


Figure 7. χ^2 maps fitting 2D DQ-DRAWS spectra of *G*GV (left), *G*FF (middle), and *V*GG (right). For each plot, one slice of a 2D χ^2 map for (ϕ, ψ) is shown with ϕ held at the best-fit value from the DQ buildup experiment and ψ varied from -180° to $+180^\circ$.

scheme was employed. In order to further decouple the $^{13}\text{C}'$ spins from the proton bath during the DRAWS periods, a z -filter was inserted between the cross polarization and DRAWS modules by storing the carbon magnetization along $-\text{I}_z$ and dropping the proton field to 25 kHz for two rotor periods. An additional rotor echo was placed at the end of the pulse sequence to allow direct comparison between DQ-filtered spectra and CP/MAS spectra (an echo is used in the CP experiment to minimize background signal from the probe).

The numerical simulations incorporated explicit input parameters for the rf fields, the CSAs, the dipolar coupling, and Euler angles to orient the interactions into a common reference frame. In simulating both the DQ buildup and 2D DQ-CSA data a sufficient number of crystallites must be used. In particular these sequences are not γ -independent so a combina-

tion of 114 α , β angles obtained using the repulsion algorithm⁶⁷ with 14 random γ angles were used. Lower numbers of α , β , γ angles gave qualitatively good results but did not reproduce the high-frequency sideband intensities as well. The Euler angles for orienting the dipolar interaction are dependent on the vector connecting the carbonyl carbons in the reference frame. $^{13}\text{C}'$ CSAs have been determined to adopt reasonably uniform orientations with respect to the amide bonds; however, there is some variability in the orientation of σ_{11} and σ_{22} relative to the $\text{C}'\text{-N}$ bond. In initial calculations the commonly employed values from Teng and Cross⁶² were used, but later calculations showed improvement in the fit of the 2D DQ-CSA data to crystallographic values when the angle between σ_{22} and the $\text{C}'\text{-N}$ bond was held at 37° for samples with extended conformations and 42° for samples with helical conformations. Further adjustments to the CSA tensor values based on the

(67) Bak, M.; Nielsen, N. C. *J. Magn. Reson.* **1997**, *125*, 132–139.

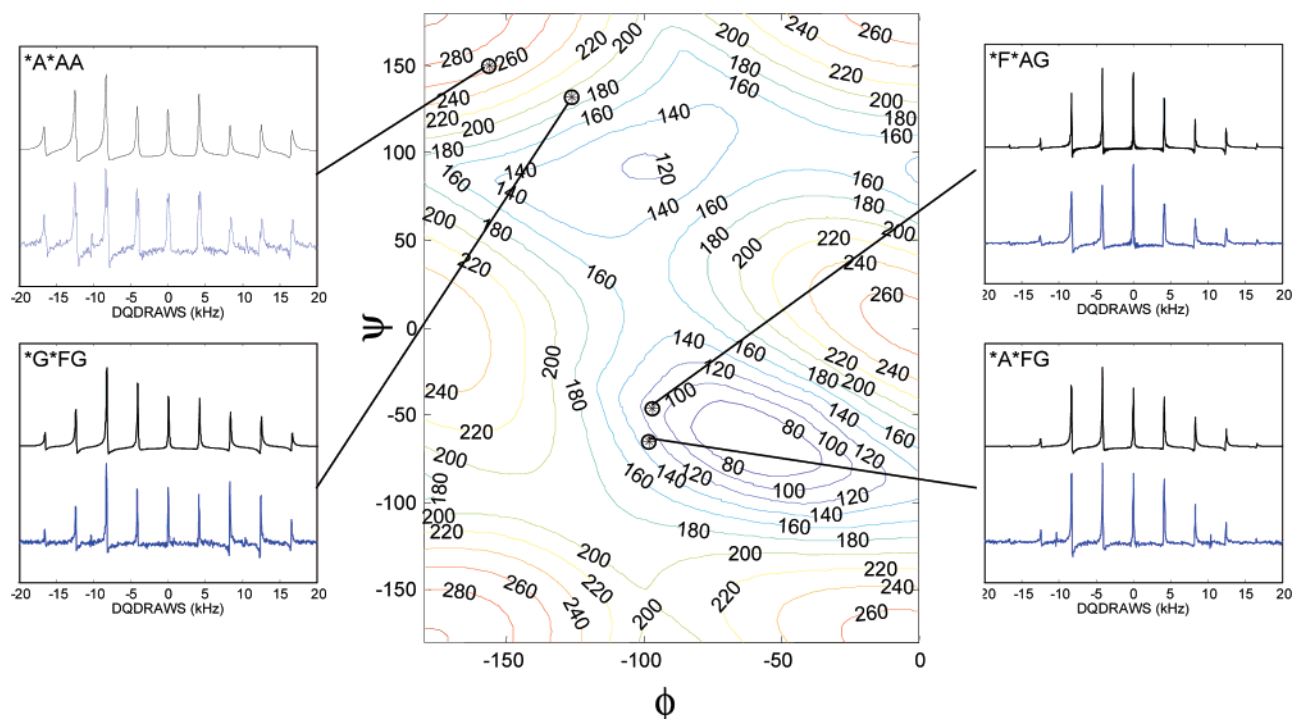


Figure 8. Contour plot showing the variation in the span of the tensorial sum of the two carbonyl carbon CSAs ($\Delta\sigma_{DQ}$) with ϕ and ψ . (Insets) Examples of the resulting DQ spectra for representative conformations. Blue spectra are experimental data, and black spectra are simulations that best fit the data.

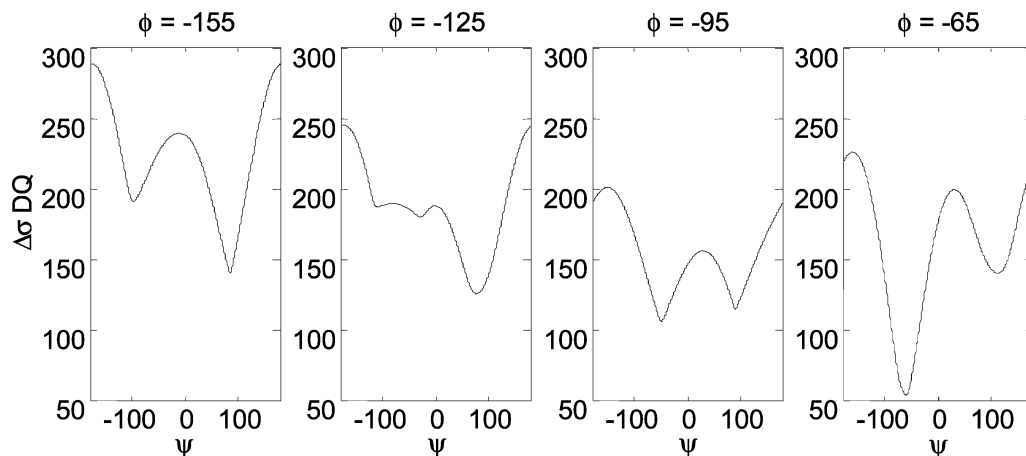


Figure 9. Variation of $\Delta\sigma_{DQ}$ with ψ for ϕ values as marked.

isotropic chemical shifts and CSA orientations based on the type of secondary structure led to the best fits given in Table 2. In addition to χ^2 maps generated using sample-dependent parameters, fits using more general parameters are presented in the Supporting Information. It should be emphasized that, with the generalized parameters, simulations fit the 2D DQ-CSA data to within 10° of the refined simulations. Previously, numerical simulations which explicitly incorporated single quantum and DQ T_2 relaxation into the calculations were done, at the cost of significantly increasing the computational time. In this work, calculations were done using the widely available and standardized SIMPSON⁶⁴ programming platform, which at this time does not allow for explicit incorporation of relaxation into the calculations. However, the omission of relaxation rates proved to be a nonissue, as by ensuring the homogeneity of the ^{13}C rf field and having a significant power mismatch between the ^{13}C and ^1H rf fields there is no need to rely on the theoretically dubious use of DQ relaxation rates. Typical ^{13}C single quantum

relaxation times are on the order of 6 ms, and applying this 50 Hz damping exponential to the simulated DQ buildup curves was sufficient for them to match the experimental data. Furthermore, omitting relaxation in the 2D DQ-CSA simulations was not detrimental to their accuracy in fitting backbone torsion angles.

In applying these techniques to less ideal, more heterogeneous samples where natural abundance background signals preclude deconvolution of CP/MAS spectra and make corrections of SQ signal intensities difficult, the accuracy of the DQ experiments will nonetheless be unaffected. Coherence selection allows for unequivocal assignment of the isotropic chemical shifts and measurement of signal intensities. Solely on the basis of the isotropic chemical shifts and signal intensities one can calculate the individual ^{13}C CSAs and perform iterative fitting to determine both ϕ and ψ to the same accuracy as presented here. The one caveat is that care must be taken to ensure dynamics do not affect signal intensities or the breadth of the CSAs.

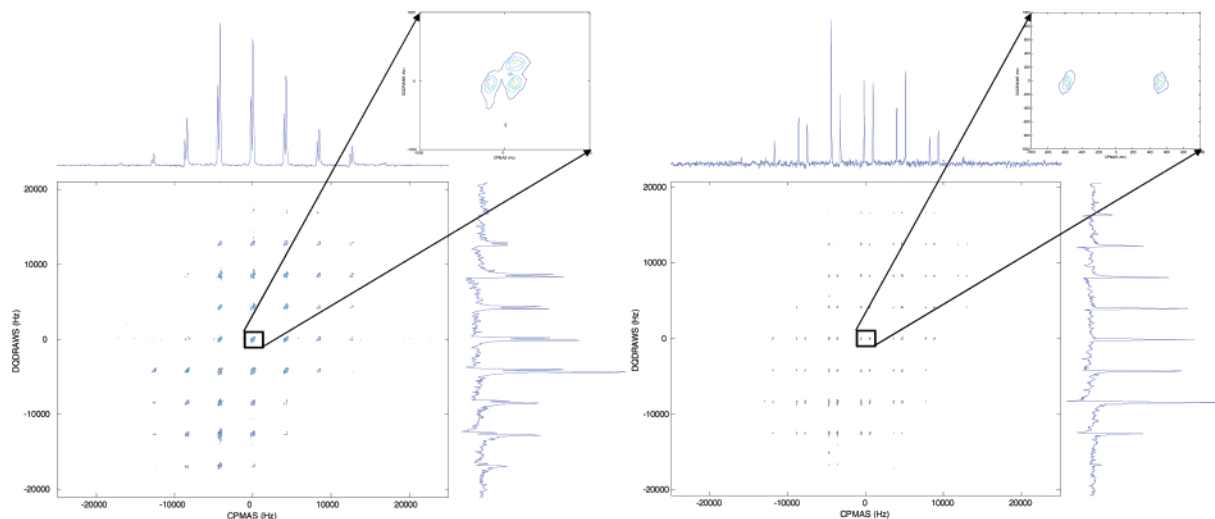


Figure 10. Comparison of a single conformation vs multiple conformations. On the left is shown the 2D DQ-CSA spectrum for $^*A^*GG$ which contains two polymorphs, resulting in a splitting seen for the peaks in the DQ dimension. On the right is shown a 2D DQ-CSA spectrum for $^*G^*FF$. Although the $^{13}C'$ single quantum chemical shifts for $^*G^*FF$ are well resolved, leading to separate resonances in the DQ filtered f_2 dimension, a single conformation leads to a single resonance in the f_1 dimension.

The tripeptide samples analyzed in this work were all polycrystalline, but in most condensed phases (such as fully solvated states, interfacial regions, and membrane environments) crystalline order is absent, and oftentimes a distribution of conformations is present. Small molecules in particular tend to exhibit discrete conformational minima in the potential energy surface, which correspond to distinct structures. It would be desirable to be able to detect multiple conformations in such cases, and a sensitive structure determination method should be able to detect such heterogeneity. The 2D DQ-DRAWS technique is capable of distinguishing between multiple secondary structures. A test case came about after an attempt to recrystallize the tripeptide AGG resulted in an unintended crystalline polymorph exhibiting two different species. The 2D DQ-CSA spectrum of this sample clearly shows two interlaced spectral patterns (Figure 10). Interestingly, this difference is more likely due to a variation in hydrogen-bonding rather than backbone secondary structure as X-ray crystallography did not detect a second conformation (CCDC 252455; complete lists of bond lengths, angles, and torsion angles are available free of charge via www.ccdc.cam.ac.uk/conts/retrieving.html),⁶⁸ and the 2D DQ-CSA data fit to the same ϕ, ψ conformations. These results also demonstrate that 2D DQ-CSA experiments would be capable of assigning torsion angles for multiple conformations in the same sample if sufficient resolution exists in the DQ dimension.

5. Conclusion

This work has demonstrated the applicability of the DQ-DRAWS technique for the determination of peptide secondary structure in the solid state. The results show that this suite of experiments is compelling for several reasons. One, DQ-DRAWS is efficacious at generating homonuclear DQ coherences at relatively high magnetic field strengths by suppressing chemical shift anisotropies. The ability of DQ-DRAWS to do so represents a significant component of its success. In fact we

have recently been able to collect 2D DQ-CSA data at 900 MHz with fairly good efficiency (data not shown).

Two, using DQ-DRAWS, the buildup of DQ coherence between adjacent $^{13}C'$ spins in a peptide yields highly accurate values of the torsion angle ϕ over a broad range of possible geometries. The behavior of the DQ coherence generated between these spins can be used to determine highly accurate values of both ϕ and ψ over a broad range of secondary structures, regardless of hydrogen-bonding effects, demonstrating the reasonable possibility of using one experiment over a full range of secondary structures.

Three, the numerical simulations required to extract the dihedral angles from the experimental data can be performed using commonly available packages (such as SIMPSON,⁶⁴ SIMMOL,⁶⁹ and SPINEVOLUTION⁷⁰) on a typical single-processor machine in a reasonable amount of time using canonical bond lengths and bond angles for peptide geometries. The determination of the backbone dihedral angles does not require a priori structural knowledge of the system at hand. The DQ-CSA analysis presented earlier shows that an inference can be drawn about the geometry from the envelope of spinning side bands in the pure DQ spectrum, even before embarking on any numerical simulation.

Four, the DQ-DRAWS experiment is able to give accurate results over a range of magnetic field strengths, under moderate sample spinning and rf conditions and standard commercial NMR spectrometers. Also, the DQ-DRAWS experiment does not require any natural abundance correction of the data since DQ excitation serves as a built-in filter for background signal.

Five, the technique described and demonstrated here does not require exotic or extensive isotopic labeling. The isotropic labeling scheme is constant, regardless of secondary structure, and hence no independent information regarding the conformation of the protein is needed to select labels. For peptides that are amenable to solid-phase chemical synthesis, the $^{13}C'$ labels can be easily incorporated using commonly available amino

(68) Zeller, M.; Mills, F.; Long, J. R.; Mehta, M. A.; Hunter, A. D. Cambridge Crystallographic Data Centre (CCDC): Cambridge, UK, 2004; crystal coordinates for AGG, unit cell parameters: $a = 7.7750(8)$ Å, $b = 5.3753(6)$ Å, $c = 12.1491(13)$ Å, $\beta = 102.836(2)^\circ$, space group $P2_1$.

(69) Bak, M.; Schultz, R.; Vosegaard, T.; Nielsen, N. C. *J. Magn. Reson.* **2002**, *154*, 28–45.

(70) Veshkort, M.; Griffin, R. G. *J. Magn. Reson.* **2006**, *178*, 248–282.

acids, as was done for the samples studied here. For larger molecular systems, the isotopic labeling arrangements required for DQ-DRAWS are amenable to protein expression using *Escherichia coli* and selecting unique pairs of adjacent amino acids.⁶³

Even though the work presented here has focused on microcrystalline samples, it should be emphasized that the applicability of the DQ-DRAWS technique can be extended to solid states lacking long-range order.^{5,71} The integrity of the experiment is uncompromised for samples in amorphous or glassy states, and may in fact yield important structural information when only local order is present, albeit for unresolved resonances the information would be more qualitative than quantitative. Furthermore, reliable performance at high magnetic field strengths makes it possible to detect simultaneous, multiple conformations at ambient conditions. The homonuclear DQ excitation between dipole-coupled nuclei makes it practicable to interrogate dilute molecular systems in the presence of large, heterogeneous backgrounds, such as membranes, solid supports, protein assemblies, and other matrices. These techniques can also be applied to more extensively labeled samples although the ability to accurately measure specific interactions would be somewhat diminished, as is true for all recoupling sequences unless one has very well-resolved resonances and

can apply them in a frequency-selective manner. While the DQ-DRAWS is not appropriate for solving entire protein structures, it can play an important role in the arsenal of techniques being developed for protein structure determination via ssNMR and should be utilized for answering mechanistic questions requiring the highest-resolution structural data.

Acknowledgment. We thank Nathan Oyler for Matlab subroutines used in processing and simulating the NMR data. Numerical simulations were performed at the University of Florida High-Performance Computing Center and the Oberlin cluster. We thank Matthias Zeller and Allen Hunter of Youngstown State University for their assistance with the single-crystal structure determination of several peptides. Support from NSF-CAREER Grant CHE-0449629 (MAM), NSF-MRI Grant CHE-0079470 toward acquisition of the Oberlin 600 MHz NMR spectrometer, NSF-MRI Grant CHE-0420717 toward the acquisition of the Oberlin parallel computational cluster, the NSF National High Magnetic Field Laboratory (S.A.M.), Research Corporation (M.A.M.), University of Florida (J.R.L.), and Oberlin College (M.T.E.) is gratefully acknowledged.

Supporting Information Available: Details of the NMR experiments and numerical simulations as well as data for all the compounds. This material is available free of charge via the Internet at <http://pubs.acs.org>.

(71) Mehta, M. A.; Fry, E. A.; Eddy, M. T.; Dedeo, M. T.; Anagnost, A. E.; Long, J. R. *J. Phys. Chem. B* **2004**, *108*, 2777–2780.

JA074244W